

On the rapidly cooling interior of supergalactic winds

S. Silich^{1,2}, G. Tenorio-Tagle¹ and C. Muñoz-Tuñón³

ABSTRACT

Here we present the steady state numerical solution and two dimensional hydrodynamic calculations of supergalactic winds, taking into consideration strong radiative cooling. The two possible outcomes: quasi-adiabatic and strongly radiative flows are thoroughly discussed, together with their implications on the appearance of supergalactic winds both in the X-ray and visible line regimes.

Subject headings: Galaxies: superwinds, Starbursts: optical and X-ray emissions, general - starburst galaxies

1. Introduction

Massive starbursts, well localized short episodes of violent star formation, are among the intrinsic characteristics of the evolution of galaxies. They are found both at high and intermediate redshifts (Dawson et al., 2002; Ajiki et al., 2002; Pettini et al., 1998) as well as in galaxies in the local universe (Marlowe et al., 1995, Cairos et al., 2001).

It has usually been assumed that the energy deposition occurs within a region of about 100 pc, the typical size of a starburst. However recent optical, radio continuum and IR observations (Ho 1997; Johnson et al. 2001, Gorjian et al. 2001) revealed a number of unusually compact young stellar clusters. These overwhelmingly luminous concentrations of stars present a typical radius of about 3 pc, and a mass that ranges from a few times $10^4 M_{\odot}$ to $10^6 M_{\odot}$. Clearly these units of star formation (super-star clusters) are very different from what was usually assumed to be a typical starburst, and we shall put a special emphasis on the outflows expected from them.

The large kinetic luminosity produced by violent bursts of star formation is well known to drastically affect the surrounding interstellar medium,

generating the giant superbubbles and supershells, detected in a large sample of star-forming galaxies (Bomans, 2001). In other cases, the energy input rate is able to drive their associated shock waves to reach the outskirts of their host galaxy, leading, in these cases, to the development of a supergalactic wind with outflow rates of up to several tens of solar masses per year (see Heckman 2001 for a complete review). One of the main implications of such outflows is the clear contamination of the intergalactic medium with the metals recently processed by the massive starburst. In both cases it is usually assumed that at the heart of the starburst, within the region that encompasses the recently formed stellar cluster (R_{SB}), the matter ejected by strong stellar winds and supernova explosions is fully thermalized. This generates the large central overpressure responsible for the mechanical luminosity associated with the new starburst. Within the starburst region, it is the mean total mechanical energy L_{SB} and mass \dot{M}_{SB} deposition rates that control, together with the actual size of the star forming region R_{SB} , the properties of the resultant outflow. The total mass and energy deposition rates define the central temperature T_{SB} and thus the sound speed c_{SB} at the cluster boundary. As shown by Chevalier & Clegg (1985; hereafter referred to as CC85) at the boundary $r = R_{SB}$, the thermal and kinetic energy flux amount exactly to 9/20 and 1/4 of the

¹Instituto Nacional de Astrofísica Óptica y Electrónica, AP 51, 72000 Puebla, México

²Main Astronomical Observatory National Academy of Sciences of Ukraine, 03680, Kiev-127, Golosiiv, Ukraine

³Instituto de Astrofísica de Canarias, E 38200 La Laguna, Tenerife, Spain

total energy flux:

$$F_{th}/F_{tot} = \frac{\frac{1}{\gamma-1} \frac{P}{\rho}}{\frac{u^2}{2} + \frac{\gamma}{\gamma-1} \frac{P}{\rho}} = \frac{9}{20}, \quad (1)$$

$$F_k/F_{tot} = \frac{u^2/2}{\frac{u^2}{2} + \frac{\gamma}{\gamma-1} \frac{P}{\rho}} = \frac{1}{4}. \quad (2)$$

There is however a rapid evolution as matter streams away from the central starburst. After crossing $r = R_{SB}$ the gas is immediately accelerated by the steep pressure gradients and rapidly reaches its terminal velocity ($V_\infty \approx 2 c_{SB}$). This is due to a fast conversion of thermal energy, into kinetic energy in the resultant wind. In this way, as the wind takes distance to the star cluster boundary, its density, temperature and thermal pressure will drop as r^{-2} , $r^{-4/3}$ and $r^{-10/3}$, respectively (CC85). Previous analysis by Heckman et al. (1990) showed that thermal pressure radial distributions inside starburst galaxies M82 and NGC 3256 are in a good agreement with the CC85 model. However Martin et al. (2002) found that X-ray surface brightness and radial temperature gradient observed by Chandra in NGC 1569 are inconsistent with CC85 predictions.

Note that the wind is exposed to the appearance of reverse shocks whenever it meets an obstacle cloud or when its thermal pressure becomes lower than that of the surrounding gas, as is the case within superbubbles. There, the high pressure acquired by the swept up ISM becomes larger than that of the freely expanding "free wind region" (FWR), a situation that rapidly leads to the development of a reverse shock, the thermalization of the wind kinetic energy and to a much reduced size of the FWR. Thus for the FWR to extend up to large distances away from the host galaxy, the shocks would have had to evolve and displace all the ISM, leading to a free path into the intergalactic medium and to a supergalactic wind with properties similar to those derived by CC85. Here we study the true physical properties of such well developed FWRs, taking into consideration strong radiative cooling. Section 2 compares the adiabatic solution of CC85 with our steady state solution where radiative cooling is considered. In section 2 we also develop an easy criterion to define in which cases radiative cooling is to become dominant. Section 3 displays two dimensional calculations that use CC85 as the initial condition

which evolves until a new steady state is reached. Section 4 discusses some of the observational consequences of such outflows.

2. The steady state solution

Following CC85 we assume a spherically symmetric wind, unaffected by the gravitational pull caused by the central star cluster or its associated dark matter component. The equations that govern the steady outflow away from the star forming region are:

$$\frac{1}{r^2} \frac{d}{dr} (\rho u r^2) = 0, \quad (3)$$

$$\rho u \frac{du}{dr} = -\frac{dP}{dr}, \quad (4)$$

$$\frac{1}{r^2} \frac{d}{dr} \left[\rho u r^2 \left(\frac{u^2}{2} + \frac{\gamma}{\gamma-1} \frac{P}{\rho} \right) \right] = -Q, \quad (5)$$

where r is the spherical radius, $u(r)$, $\rho(r)$ and $P(r)$ are the wind velocity, density and thermal pressure, respectively. Q is the cooling rate ($Q = n^2 \Lambda$, where n is the wind number density and Λ is the interstellar cooling function, Raymond et al. 1976). At the boundary of the star cluster (R_{SB}) we use the solution of CC85

$$\dot{M}_{SB} = (0.1352\pi\gamma)^2 \frac{L_{SB}}{c_{SB}^2}, \quad (6)$$

$$P = 0.0338 \dot{M}_{SB}^{1/2} L_{SB}^{1/2} R_{SB}^{-2}, \quad (7)$$

$$T = \frac{0.299\mu}{k} \frac{L_{SB}}{\dot{M}_{SB}}, \quad (8)$$

$$u = c_{SB} = \left(\frac{\gamma k T}{\mu} \right)^{1/2}, \quad (9)$$

$$\rho = \frac{\dot{M}_{SB}}{4\pi R_{SB}^2 c_{SB}}, \quad (10)$$

where μ is the mean mass per wind particle, k is the Boltzmann constant, $\gamma = 5/3$ is the ratio of specific heats and c_{SB} is the sound speed at $r = R_{SB}$, and then solve equations (3)-(5) numerically. Note that at $r = R_{SB}$ the wind Mach number $M_w = 1$. Therefore we use the wind velocity as an independent variable at the vicinity of the sonic point. Our numerical solutions for $Q = 0$, fully reproduce CC85 adiabatic results.

2.1. Radiative cooling in supergalactic winds

A first order of magnitude estimate of whether or not radiative cooling could affect the thermodynamics of superwinds, results from a comparison of the radiative cooling time scale

$$\tau_{cool}(r) = \frac{3kT}{n\Lambda}, \quad (11)$$

with the characteristic dynamical time scale

$$\tau_{dyn}(r) = \int_{R_{SB}}^r \frac{dr}{u(r)}. \quad (12)$$

The wind density, which, as it streams away, decreases as $(1/r^2)$, in combination with the interstellar cooling curve, fully define locally the ratio of τ_{cool}/τ_{dyn} . One can infer then that if the ratio of the above two quantities becomes smaller than 1, radiative cooling sets in, affecting the thermodynamical properties of the flow. These simple estimates indicate that radiative cooling may become more efficient the more compact a star cluster is. In fact, it is the density of the free wind what really matters. For the same total starburst energy, the more compact a starburst is, the larger the wind density value and thus the larger the cooling rate. The temperature profiles for a 10^{41} erg s^{-1} starburst with a radius $R_{SB} = 5$ pc and different metallicities of the wind material are shown in Figure 1, for both the adiabatic and the radiative cases. Note that for compact starbursts radiative cooling sets in within a radius $\leq 10 R_{SB}$. Despite the rapid drop in temperature the velocity and the density distributions remain almost unaffected by radiative cooling. In all cases the thermal energy is rapidly transformed into kinetic energy of the wind in the close vicinity of the sonic point. This leads to a fast gas acceleration that allows the wind gas to rapidly approach its terminal velocity $V_{\infty} \approx 2 c_{SB}$. At the same time, if radiative cooling is considered, the temperature profile strongly deviates away from the adiabatic solution forcing the gas to soon reach temperature values of the order of 10^4 K.

One can establish an approximate boundary that separates the adiabatic from the strongly radiative cases, from the condition that τ_{cool} becomes equal to τ_{dyn} . The corresponding curves for different energy input rates, wind terminal velocities and wind metallicities, as a function of R_{SB} ,

are shown in Figure 2. If the initial wind parameters (L_{SB} and R_{SB}) intersect below the corresponding metallicity curve, cooling will be inefficient and deviations from the adiabatic solution would be negligible. On the other hand, if the initial wind parameters intersect above the corresponding metallicity curve, radiative cooling is expected to become important. Note that the larger the wind terminal velocity is, the smaller the region of the parameter space covered by the cold wind solution.

3. The time dependent solution

Several two dimensional calculations using CC85 as the initial condition adiabatic flows have been performed with the Eulerian code described by Tenorio-Tagle & Muñoz Tuñon (1997, 1998). This has been adapted to allow for the continuous injection in the most central zones, of winds with a variety of L_{SB} and \dot{M}_{SB} values. The time dependent calculations also account for radiative cooling and display the evolution from the adiabatic regime to the more realistic final steady state solution when radiative cooling is considered. There is an excellent agreement between the time dependent calculations and the steady state solutions displayed in section 2.

Figure 3 displays isotherm contours and the velocity field within the central 100 pc^2 of a supergalactic wind driven by an $L_{SB} = 10^{42}$ erg s^{-1} , $c_{SB} = 500 \text{ km s}^{-1}$ or a $V_{\infty} = 1000 \text{ km s}^{-1}$, emanating from an $R_{SB} = 20 \text{ pc}$. The solution for $Z = Z_{\odot}$, as expected from Figure 2, is well into the strongly radiative regime. Figure 3 shows the rapid increase in velocity from its central value to the terminal speed $\sim 2 c_{SB}$. The upper panel shows the run of temperature for the corresponding CC85 adiabatic solution, our initial condition, while the central panels depict how radiative cooling proceeds within the supersonic outflow, leading to the formation of cool parcels of gas ($T \sim 10^4$ K) within rapidly expanding shells of cooling gas. After a few 10^4 years a new steady state solution has been reached (lower panel). There the temperature of the fast moving wind suddenly plummets from 10^7 K to 10^4 K at a distance of 37 pc from R_{SB} . Cooling takes place in a catastrophic manner, a fact that made us search for possible signs of fragmentation, however, the sudden pressure gra-

dients resulting from cooling are inhibited by the strongly diverging flow, leaving both the density and the velocity fields almost unperturbed. Similar results were obtained when higher metallicity outflows were assumed. The high metallicities are indeed expected from the large inflow of new metals into the superwind (see Silich et al., 2001). Figure 4 shows the final steady-state solution for a wind with $R_{SB} = 5$ pc, $L_{SB} = 10^{41}$ erg s^{-1} and $V_{\infty} = 1000$ km s^{-1} when the assumed metallicity of the wind is equal to $1Z_{\odot}$, $3Z_{\odot}$, $5Z_{\odot}$ and $10Z_{\odot}$. Clearly the impact of this variable is to favor radiative cooling even closer to the R_{SB} surface, fact that can be also noticed in Figure 1.

4. The structure of supergalactic winds

The results from sections 2 and 3 imply that the structure of supergalactic winds ought to be revised, particularly in the case of powerful sources with a small value of R_{SB} in which radiative cooling reduces the spatial extent of the X-ray emitting region. In such cases, the only possibility for the origin of an extended hot gas component arises from shock heated ISM overrun by the central wind. On the other hand, in lower luminosity and/or widely spread starbursts, the extended hot wind region may also contribute significantly to the total soft X-ray emission. Here we center our attention on very massive and centrally concentrated starbursts, entities that leave no doubt that their newly processed elements will sooner or later be driven into the IGM. In such cases the central wind is affected by radiative cooling and the extended structure of such winds will be undetected in the X-ray regime.

Supergalactic winds present a four zone structure: 1) A central starburst region (a source of hard and soft X-rays). 2) A soft X-ray emitting zone. 3) The line cooling zone. 4) A region of recombined gas, exposed to the UV radiation from the central star cluster.

Figure 5 displays the radial structure of supergalactic winds powered by low ($L_{SB} = 10^{41}$ erg s^{-1}) and high ($L_{SB} = 10^{43}$ erg s^{-1}) luminosity starbursts as a function of R_{SB} . In all cases we have assumed a free wind region terminal velocity equal to 1000 km s^{-1} and a $1Z_{\odot}$ metal abundance. Solid lines mark the distance at which a 10^{41} erg s^{-1} superwind acquires a temperature of 5×10^5 K

and 10^4 K for an adiabatic solution. Dashed lines present the modified location of the two temperature boundaries provided by gas cooling. Dotted lines mark the position of the two temperature boundaries for energetic starbursts (10^{43} erg s^{-1}). Note that in both high and low luminosity cases we have assumed the same central temperature, and thus the same central sound velocity (c_{SB}), both cases develop the same terminal speed, leading in the adiabatic regime to the same temperature radial structure. For the low luminosity radiative cases (heavy dashed lines) significant departures from the adiabatic solution occur for highly concentrated starbursts (say $R_{SB} \leq 20$ pc) bringing the zone of rapid radiative cooling (10^4 K $\leq T \leq 5 \times 10^5$ K) closer to the starburst surface. On the other hand, the radiative solution for the energetic cases (dotted lines) shows how both temperature limits here considered move much closer to the starbursts, reducing significantly the extent of the X-ray and the line cooling zones. The effect is noticeable for all R_{SB} (from 1pc to 100 pc) values here considered, a fact that ought to be taken into account in full numerical simulations.

4.1. The impact of photo-ionization and the expected Halpaha luminosity

Figure 5 shows that powerful and compact starbursts are to be surrounded by extended, cold and fast expanding envelopes. This continuously injected halo, however, becomes an easy target of the UV photons escaping from the central star forming regions, and as it presents an R^{-2} density distribution it should be completely ionized by the stellar radiation. This is simply because the number of recombinations in such a density distribution is, as shown by Franco et al. 1990, unable to trap the ionization front. As shown in Figure 5, the size of the X-ray and line cooling zones become strongly affected by radiative cooling reducing largely their dimensions in favor of a closer development of the outer photo-ionized region 4. Note that the recombining zone 3 is also an additional source of UV photons capable of ionizing the wind outer extended halo. The number of recombinations per unit time expected in the photo-ionized, outer free wind region is:

$$\frac{dN_{rec}}{dt} = 4\pi R_4^2 n(R_4) V_w(R_4) + 4\pi\beta \int_{R_4}^{\infty} n^2(r) r^2 dr = \frac{\dot{M}_w}{\mu_a} + \frac{\beta \dot{M}_w^2}{4\pi V_t^2 \mu_a^2 R_4}, \quad (13)$$

where the first term in the right hand side refers to the number of recombinations in the rapidly cooling zone and the second one is related to the number of recombinations in the outer cold envelope (zone 4). Recombinations should lead to H α and Ly α emission. One then can estimate the H α luminosity $L_{H\alpha} = 1.36 \times 10^{-12} \dot{N}_{rec}$ (Leitherer & Heckman, 1995) and Ly α luminosity $L_{Ly\alpha} \approx 8.74 L_{H\alpha}$ (Brocklehurst, 1971). The expected H α luminosities calculated for radiative winds powered by 10^{41} erg s $^{-1}$ and 10^{43} erg s $^{-1}$ starbursts are presented in Figure 6 as a function of R_{SB} .

4.2. The X-ray luminosity

The X-ray luminosity from the hot wind with density distribution $n(r) = \dot{M}_w / 4\pi\mu_a u(r)r^2$ is

$$L_x = 4\pi \int_{R_{SB}}^{R_x} n^2 \Lambda_x(T, Z_w) r^2 dr, \quad (14)$$

where $\Lambda_x(T, Z_w)$ is the hot gas X-ray emissivity and R_x is the X-ray emission cutoff radius that corresponds to the cutoff temperature $T_{cut} \approx 5 \times 10^5$ K. This is shown in Figure 5. We then use a model velocity field $u(r)$ and the cutoff radius R_x to calculate a wind soft (0.1keV - 2.4keV) X-ray luminosity. The results of the calculations for $L_w = 10^{41}$ erg s $^{-1}$ and $L_w = 10^{43}$ erg s $^{-1}$ superwinds are shown in Figure 6. We have to conclude that the inconsistency between the free wind model predictions and observed superwind X-ray luminosities, mentioned by Strickland & Stevens (2000), becomes even larger if one takes into account the modifications provided by radiative cooling. That is, in the standard approach the free wind material itself cannot be the main source of diffuse superwind X-ray emission.

5. Conclusions

We have reanalyzed the physical properties (velocity, density and temperature) of supergalactic winds powered by a constant energy input rate,

taking radiative cooling into account. Three input parameters control the properties of the wind: the total energy input rate L_{SB} , the characteristic scale of star formation (R_{SB}), and a thermalized gas temperature T_{SB} (or initial wind velocity c_{SB}). We have revealed two possible outflow regimes: a hot wind, which due to its low power and low density remains unaffected by cooling, and thus as found by CC85 behaves adiabatically. On the other hand, winds driven by powerful and/or compact starbursts become rapidly dominated by catastrophic radiative cooling.

Superwinds driven by compact and powerful starbursts (see Figure 2) undergo catastrophic cooling close to their sources, and establish a temperature distribution radically different from those obtained in adiabatic calculations. At the same time, both velocity and density radial distributions remain almost unchanged given the speed of the rapidly diverging flow.

The rapid fall in temperature as a function of r reduces the size of the zone radiating in X-rays and decreases the superwind X-ray luminosity. At the same time, cooling brings the 10^4 K boundary closer to the wind center, and promotes the establishment of an extended ionized fast moving envelope. This should show up as a weak and broad (~ 1000 km s $^{-1}$) line emission component at the base of the much narrower line caused by the central HII region.

The authors highly appreciated the friendly hospitality of A. D'Ercole, F. Brighenti, M. Tosi and F. Matteucci at the superwind 2002 workshop in Bologna, where this study was initiated. They thank the referee for helpful comments and Jeff Wagg for his careful reading of the manuscript. This study has been supported by CONACYT - México, research grant 36132-E and by the Spanish Consejo Superior de Investigaciones Científicas, grant AYA2001 - 3939.

REFERENCES

- Ajiki, M., Taniguchi, Y., Murayama, T. et al. 2002, ApJ, 576, L25
- Bomans, D. 2001, Rev. Mod. Astroph., 14, 297
- Brocklehurst, M., 1971, MNRAS, 153, 471
- Chevalier, R.A. & Clegg, A.W. 1985, Nature, 317, 44

- Dawson, S., Spinrad, H., Stern, D., Dey, A., van Breugel, W., de Vries, W. & Reuland, M., 2002, *ApJ*, **570**, 92
- Cairos, L.M., Caon, N., Vilches, J.M., González-Pérez, J.N. & Muñoz-Tuñón, C., 2001, *ApJS*, **136**, 393
- Franco, J., Tenorio-Tagle, G. & Bodenheimer, P., 1990, *ApJ*, **349**, 126
- Gorjian, V., Turner, J.L. & Beck, S.C. 2001, *ApJ*, **554**, L29
- Ho, L. C. 1997, *Rev.MexAA*, Conf. Ser. 6, 5
- Heckman, T.M. 2001, in *ASP Conf. Ser. 240, Gas and Galaxy Evolution*, ed. J. E. Hibbard, M. Rupen & J. H. van Gorkom (San Francisco: ASP), 345
- Heckman, T.M., Armus, L. & Miley, G.K., 1990, *ApJS*, **74**, 833
- Johnson, K. E., Kobulnicky, H. A., Massy, P. & Conti, P. S. 2001, *ApJ* **559**, 864
- Leitherer, C. & Heckman, T.M., 1995, *ApJS*, **96**, 9
- Marlowe, A. T., Heckman, T. M., Wyse, R. F. G. & Schommer, R., 1995, *ApJ*, **438**, 563
- Martin, C.L., Kobulnicky, H.A. & Heckman, T.M., 2002, *ApJ*, **574**, 663
- Pettini, M., Kellogg, M., Steidel, C., Dickinson, M., Adelberger, K. & Giavalisco, M. 1998, *ApJ*, **508**, 539
- Raymond, J. C., Cox, D. P. & Smith, B. W. 1976, *ApJ*, **204**, 290
- Silich, S.A., Tenorio-Tagle, G., Terlevich R., Terlevich E. & Netzer H., 2001, *MNRAS*, **324**, 191
- Strickland, D.K. & Stevens, I. R., 2000, *MNRAS*, **314**, 511
- Tenorio-Tagle, G. & Muñoz-Tuñón, C. 1997, *ApJ*, **478**, 134
- Tenorio-Tagle, G. & Muñoz-Tuñón, C. 1998, *MNRAS*, **293**, 299

Fig. 1.— The intrinsic temperature profile of superwinds. The dash-dotted line shows the temperature distribution derived from the adiabatic solution of CC85. Other curves show the effects of radiative cooling for different superwind metallicities.

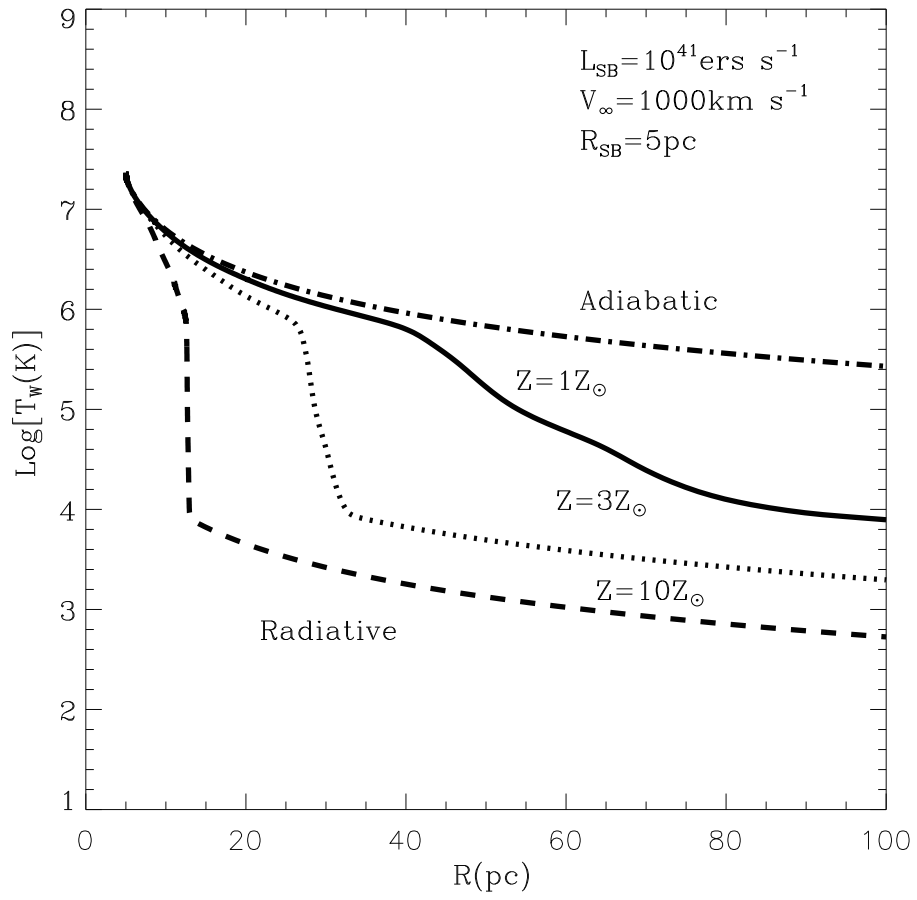
Fig. 2.— Adiabatic versus radiative superwinds. The lines divide the region defined by the parameter space into strongly radiative superwinds (above the lines) and adiabatic solutions (below the lines), for different values of the terminal velocity (V_∞) and metallicity.

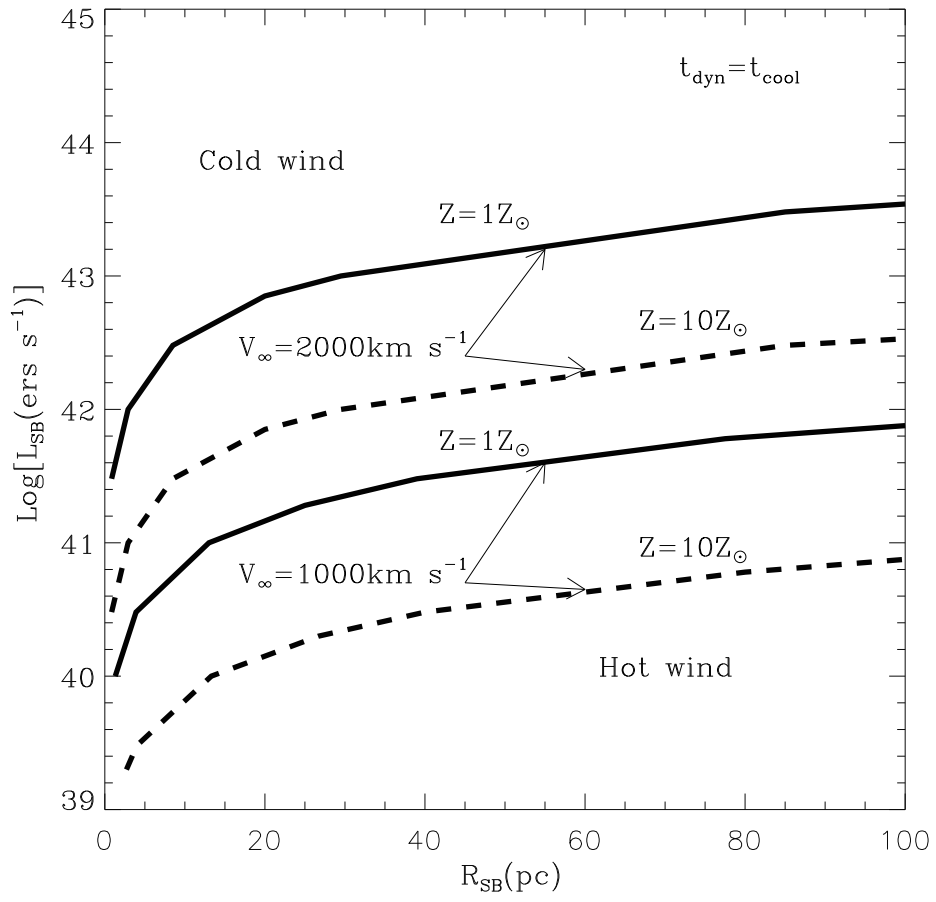
Fig. 3.— Two dimensional superwinds. Isotemperature contours, with a separation $\Delta \log T = 0.1$ and the velocity field (longest arrow = 1000 km s^{-1}) within the central 100 pc^2 of a superwind powered by a $10^{42} \text{ erg s}^{-1}$ starburst with a radius $R_{SB} = 20 \text{ pc}$. The evolution starts from (a) the adiabatic solution of CC85 and continues at (b) $t = 1.3 \times 10^4 \text{ yr}$, (c) $1.6 \times 10^4 \text{ yr}$ and (d) $1.9 \times 10^4 \text{ yr}$ when a new steady state solution is reached. In the bottom panel the gas temperature falls to 10^4 K before reaching 40 pc from the center. Distance between consecutive tick mark = 25 pc in all figures.

Fig. 4.— The metallicity effects. The same as figure 3 for a $10^{41} \text{ erg s}^{-1}$ superwind with an $R_{SB} = 5 \text{ pc}$. The panels show the final temperature and velocity distributions for the radiative steady state solution for (a) $Z = Z_\odot$, (b) $3Z_\odot$, (c) $5Z_\odot$ and (d) $10Z_\odot$.

Fig. 5.— The internal structure of free wind regions. Solid lines mark the distance at which a $10^{41} \text{ erg s}^{-1}$ superwind, with a velocity $V_\infty = 1000 \text{ km s}^{-1}$, acquires a temperature of $5 \times 10^5 \text{ K}$ and 10^4 K as a function of the initial radius R_{SB} , for an adiabatic solution. Dashed lines present the modified location of the two temperature boundaries provided by gas cooling ($Z = Z_\odot$). Dotted lines mark the position of the two temperature boundaries for energetic starbursts ($10^{43} \text{ erg s}^{-1}$).

Fig. 6.— Observational appearance of free wind regions. The expected X-ray and H_α luminosity of superwinds as a function of the starburst power and the radius R_{SB} .





This figure "silich3.jpeg" is available in "jpeg" format from:

<http://arxiv.org/ps/astro-ph/0303235v1>

